Structure, mechanical properties and corrosion resistance of nanocomposite coatings deposited by PVD technology onto the X6CrNiMoTi17-12-2 and X40CrMoV5-1 steel substrates

K. Lukaszkowicz · J. Sondor · A. Kriz · M. Pancielejko

Abstract This article presents the research results on the structure and mechanical properties of nanocomposite coatings deposited by PVD methods on the X6CrNiMoTi17-12-2 austenitic steel and X40CrMoV5-1 hot work tool steel substrates. The tests were carried out on TiAlSiN, CrAlSiN and AlTiCrN coatings. It was found that the structure of the PVD coatings consisted of fine crystallites, while their average size fitted within the range 11–25 nm, depending on the coating type. The coatings demonstrated columnar structure and dense cross-sectional morphology as well as good adhesion to the substrate, the latter not only being the effect of adhesion but also by the transition zone between the coating and the substrate, developed as a result of diffusion and high-energy ion action that caused mixing of the elements in the interface zone. The critical load L_{C2} lies within the range 27–54 N, depending on the coating and substrate type. The coatings demonstrate a high hardness ($\sim$40 GPa) and corrosion resistance.

K. Lukaszkowicz (✉)
Institute of Engineering Materials and Biomaterials, Silesian University of Technology, Konarskiego St. 18A, 44-100 Gliwice, Poland
e-mail: krzysztof.lukaszkowicz@polsl.pl

J. Sondor
LISS a.s., Zuberska 2603, 756-61 Roznov pod Radhostem, Czech Republic

A. Kriz
Department of Materials Science and Technology, University of West Bohemia, Univerzitni 22, 306-14 Plzen, Czech Republic

M. Pancielejko
Institute of Mechatronics, Nanotechnology and Vacuum Technique, Koszalin University of Technology, Raclawicka Str. 15-17, 75-620 Koszalin, Poland

Introduction

The research issues concerning the production of coatings are the most important directions of surface engineering development, ensuring the obtainment of coatings of high usable properties in the scope of mechanical characteristics and corrosion resistance [1–5]. Giving new operating characteristics to commonly known materials is frequently obtained by laying simple monolayer, multilayer or gradient coatings using PVD methods [6, 7]. While selecting the coating material, we encounter a barrier caused by the fact that numerous properties expected from an ideal coating are impossible to be obtained simultaneously. For example, an increase in hardness and strength causes the reduction of the coating's ductility and adherence to the substrate. The application of the nanostructure coatings is seen as the solution of this issue [8, 9]. According to the Hall–Petch equation, the strength properties of the material rise along with the reduction of the grain size. In case of the coatings deposited in the PVD processes, the structures obtained with grain size $\sim$10 nm cause the obtainment of the maximum mechanical properties. Coatings of such structure present very high hardness >40 GPa, ductility, stability in high temperatures, etc. [10–12].

The known dependency between the hardness and abrasion resistance became the foundation for the development of harder and harder coating materials. The progress in the field of producing coatings in the physical vapour deposition process enables the obtainment of coatings of nanocrystal structure presenting high mechanical and usable properties. The coatings of such structure are able to maintain a low friction coefficient (self-lubricating coatings) in numerous working environments, maintaining high hardness and increased resistance [13, 14].

The main concept in the achievement of high hardness of nanostructure coatings and good mechanical properties and high strength related to it, particularly in case of nanocomposite coatings [15–17], is the restriction of the rise and the movement of dislocations. High hardness and strength of the nanocomposite coatings are due to the fact that the movement of dislocations is suppressed at small grains and in the spaces between them, which causes the appearance of incoherent deformations. When the grain size is reduced to that of nanometres, the activity of dislocations as the source of the material ductility is restricted. This type of coatings is also characterized with a large number of grain boundaries with a crystalline/amorphous transition across grain–matrix interfaces, restricting the rise and development of cracks. Such mechanism explains the resistance to fragile cracking of nanocomposite coatings [18–20]. Simultaneously, the equiaxial grain shapes, high angle grain boundaries, low surface energy and the presence of the amorphous boundary phase facilitating the slide along the grain boundaries cause a high plasticity of the nanocomposite coatings [8].

Nanocomposite coatings comprise at least two phases, a nanocrystalline phase and a matrix phase, where the matrix can be either nanocrystalline or amorphous phase. Various analyses revealed that the synthesized TiAlSiN coatings exhibited nanostructured composite microstructures consisting of solid-solution (Ti,Al,Si)N crystallites and amorphous Si_3N_4. The Si addition caused the grain refinement of (Ti,Al,Si)N crystallites and its uniform distribution with percolation phenomenon of amorphous silicon nitride [11, 15–17].

One of the general reasons for depositing by PVD techniques is that protective coatings deposited by PVD tend to have higher corrosion resistance than the substrate material. Ceramic hard coatings increase the life of the coated components, not only due to the protection against aggressive environments, but also during operation involving mechanical contact with abrasive surfaces. This effect results of high hardness resulting from the smaller grain size of the coatings' structure [6].

The purpose of this article is to examine the structure, mechanical properties and corrosion resistance of nanocomposite coatings deposited by PVD technique on the X6CrNiMoTi17-12-2 austenitic stainless steel substrate and the X40CrMoV5-1 hot work tool steel substrate.

Experimental procedures

The tests were made on samples of the X40CrMoV5-1 hot work tool steel and the X6CrNiMoTi17-12-2 austenitic stainless steel, deposited by PVD process with TiAlSiN, CrAlSiN, AlTiCrN hard coatings.

Table 1 Deposition parameters of the coatings

Coating	Substrate bias voltage (V)	Arc current source (A)	Pressure (Pa)
TiAlSiN	−90	Ti—80	2.0
		AlSi—120	
CrAlSiN	−60	Cr—70	3.0
		AlSi—120	
AlTiCrN	−60	Cr—70	2.0
		AlTi—120	

The coating deposition process was made in a device based on the cathodic arc evaporation method in an Ar and N_2 atmosphere. Cathodes containing pure metals (Cr, Ti) and the AlSi (88:12 wt%) alloy were used for deposition of the coatings. The base pressure was 5×10^{-6} mbar, the deposition temperature was ∼500 °C. The deposition conditions are summarized in Table 1.

Diffraction and thin film structure were tested with the use of the JEOL JEM 3010UHR transmission electron microscope, at 300 kV bias voltage.

Observations of surface and structures of the deposited coatings were carried out on cross sections in the SUPRA 25 scanning electron microscope. Detection of secondary electron was used for generation of fracture images with 15 kV bias voltage.

Phase identification of the investigated coatings was performed by glancing angle X-ray diffraction (GAXRD).

The cross-sectional atomic composition of the samples (coating and substrate) was obtained by using a glow discharge optical spectrometer, GDOS-750 QDP from Leco Instruments. The following operation conditions of the spectrometer Grimm lamp were fixed during the tests.

- lamp inner diameter—4 mm;
- lamp supply voltage—700 V;
- lamp current—20 mA;
- working pressure—100 Pa.

Tests of the coatings' adhesion to the substrate material were made using the scratch test on the CSEM REVETEST device. The tests were made using the following parameters.

- load range 0–100 N,
- load increase rate (dL/dt): 100 N/min,
- indenter's sliding speed (dx/dt): 10 mm/min,
- acoustic emission detector's sensitivity AE: 1.

The critical load L_C, causing the loss of the coating adhesion to the material, was determined on the basis of the values of the acoustic emission, AE, and friction force, F_t and observation of the damage [21, 22] developed in the track using a LEICA MEF4A optical microscope.

The microhardness tests of coatings were made with the SHIMADZU DUH 202 ultra-microhardness tester. The test conditions were selected in order as to be comparable for all coatings. Measurements were made with 50 mN load, to eliminate the substrate influence on the coating hardness.

The thickness of coatings was determined using the ''kalotest'' method, i.e. measuring the characteristics of the spherical cap crater developed on the surface of the coated specimen tested [23].

The X-ray line broadening technique was used to determine crystallite size of the coatings using Scherrer formula [24] with silicon as internal standard.

$$D = (0.94\lambda / B\cos\theta_B) \qquad (1)$$

where D, crystallite size; B, full width at half-maximum XRD peak in radians; λ, wavelength of the X-ray radiation; θ_B the Bragg angle in radians.

Investigation of the electrochemical corrosion behaviour of the samples was done in a PGP 201 Potentiostat/Galvanostat, using a conventional three-electrode cell consisting of a saturated calomel reference electrode (SCE), a platinum counter electrode and the studied specimens as the working electrode. To simulate the aggressive media, 1-M HCl solution was used under aerated conditions and room temperature. The aqueous corrosion behaviour of the coatings was studied first by measuring the open circuit potential (OCP) for 1 h. Subsequently, a potentiodynamic polarization curve has been recorded. The curve started at a potential of ~ 100 mV below the corrosion potential and ended at $+1200$ mV or a threshold intensity level set at 100 mA/cm^2. Once this level was reached, the reverse cycle was started. The scan rate was 15 mV/min. The corrosion current densities and the polarization resistance were obtained on the basis of the Tafel analysis after potentiodynamic polarization measurements. The calculation of the corrosion rate was performed as follows.

$$\text{Corr.} = \frac{i_{\text{cor}} \cdot M}{D \cdot V} \text{ (mm/year)}$$

where i_{cor}, corrosion current density (A/cm^2); D, density (g/cm^3); M, atomic mass (g); V valence.

Results and discussion

The coatings present a compact structure, without any visible delaminations or defects. The morphology of the fracture of coatings is characterized by a dense structure, in some cases there is a columnar structure (Figs. 1, 2, 3). The fracture surface of the steel samples was examined and the deposited coatings show a sharp transition zone between the substrate and the coating.
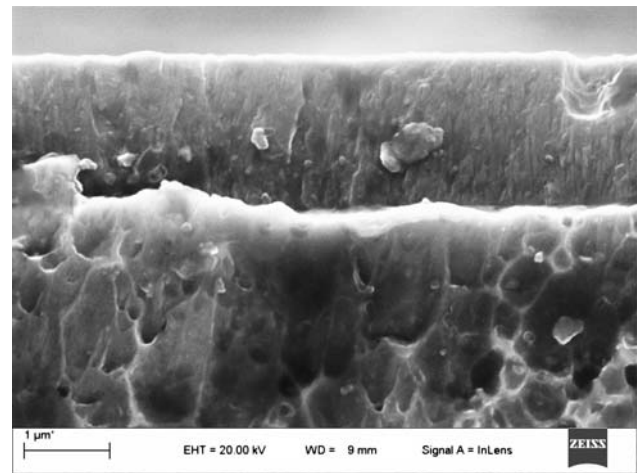

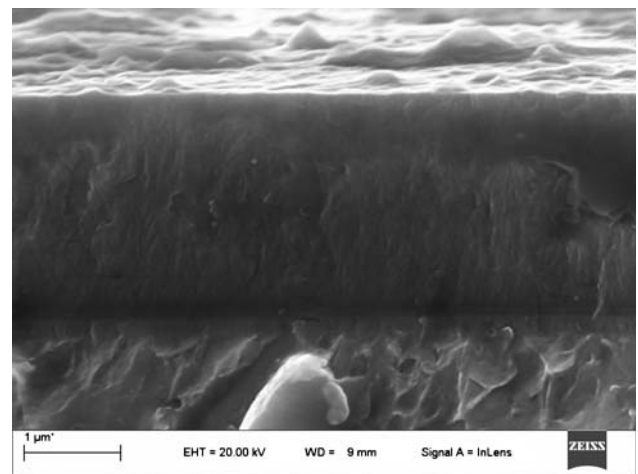**Fig. 1** Fracture of the TiAlSiN coating deposited onto the X40CrMoV5-1 steel substrate

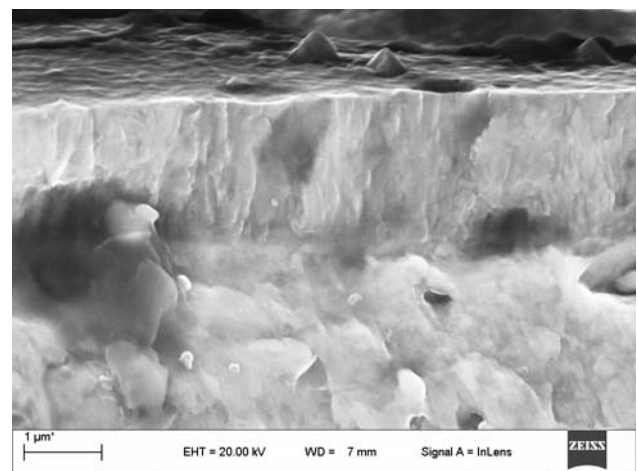**Fig. 2** Fracture of the CrAlSiN coating deposited onto the X40CrMoV5-1 steel substrate

Fig. 3 Fracture of the AlTiCrN coating deposited onto the X40CrMoV5-1 steel substrate

Fig. 4 Structure of the thin foil from the TiAlSiN coating deposited onto the austenitic steel X6CrNiMoTi17-12-2. **a** light field, **b** dark field from the (111) reflex, **c** diffraction pattern from the area as in **a**, **d** solution of the diffraction pattern
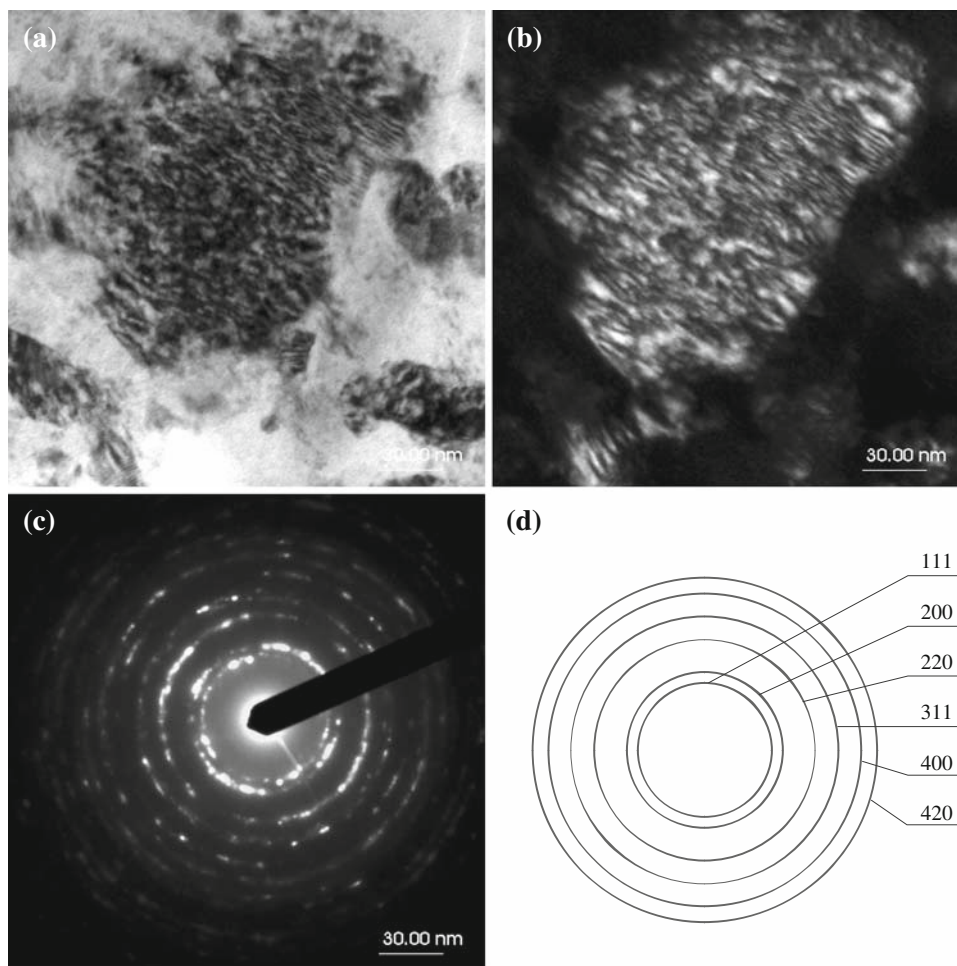
Transmission electron microscopy (TEM) examination of the coatings showed that they consisted of fine crystallites, and there was no suggestion of epitaxial growth. Single large grains were only observed in case of the TiAlSiN coating (Fig. 4), which may suggest the occurrence of the epitaxion phenomenon as the consequence of large crystallite occurrence in the coating.

Based on the glancing angle X-ray diffraction (GAXRD) of the samples examined (Figs. 5, 6, 7), the occurrence of fcc phases was only observed in the coatings. The hexagonal AlN of wurtzite type was not discovered in the coatings examined, which could have been caused by a low amount of aluminium in the coatings. Based on the results obtained, using Scherer method, the size of crystallites in the coatings examined was determined. The results were presented in Table 2.

The hardness of the coatings tested fits within the range from 40 to 42 GPa. The highest hardness was recorded in the case of the AlTiCrN coating (Table 2).

The critical load values L_{C1} and L_{C2} were determined by the scratch test method (Figs. 8, 9, 10). The load at which the first coating defects appear is known in the references
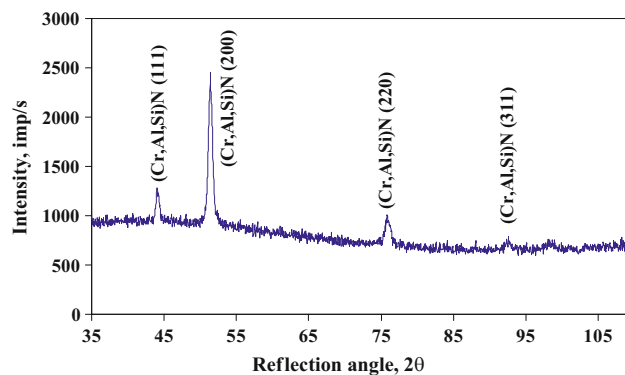

Fig. 5 GAXRD spectra of the CrAlSiN coating at glancing incidence angle $\alpha = 2°$

[25, 26] as the first critical load L_{C1}. The first critical load L_{C1} corresponds to the point at which first damage is observed; the first appearance of microcraking, surface flaking outside or inside the track without any exposure of the substrate material—the first cohesion-related failure event (Figs. 11a, 12a, 13a). L_{C1} corresponds to the first small jump on the acoustic emission signal, as well as on
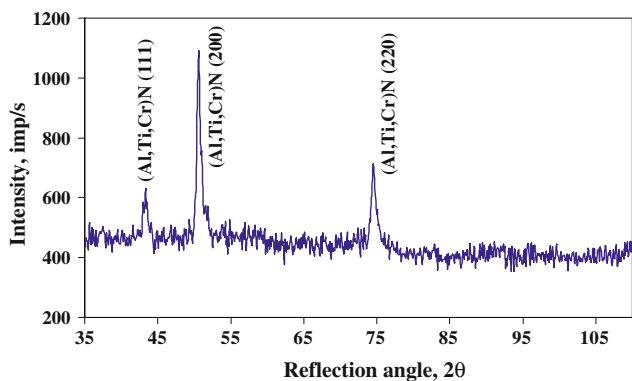
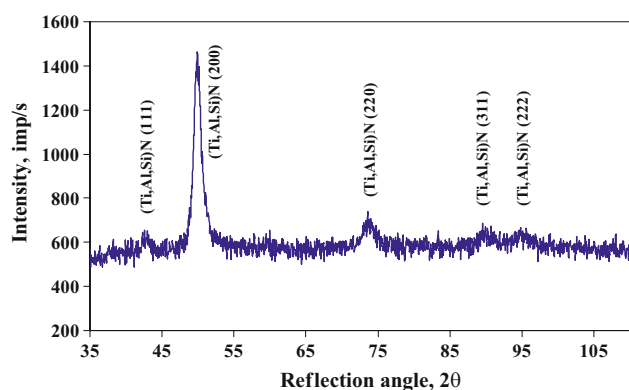**Fig. 6** GAXRD spectra of the AlTiCrN coating at glancing incidence angle $\alpha = 2°$

Fig. 8 Diagram of the dependence of the acoustic emission (AE) and friction force F_t on the load for the X40CrMoV5-1 steel with the AlTiCrN coating

Fig. 7 GAXRD spectra of the TiAlSiN coating at glancing incidence angle $\alpha = 2°$

Fig. 9 Diagram of the dependence of the acoustic emission (AE) and friction force F_t on the load for the X40CrMoV5-1 steel with the CrAlSiN coating

the friction force curve (Figs. 8, 9, 10). The second critical load L_{C2} is the point at which complete delamination of the coatings starts; the first appearance of cracking, chipping, spallation and delamination outside or inside the track with the exposure of the substrate material—the first adhesion-related failure event (Figs. 11b, 12b, 13b). After this point the acoustic emission graph and friction forces have a disturbed run (become noisier). The cumulative specification of the test results are presented in Table 2.

To establish the nature of damage causing the increase in acoustic emission intensity, the examinations of the scratches that arose during the test were made with the use of the
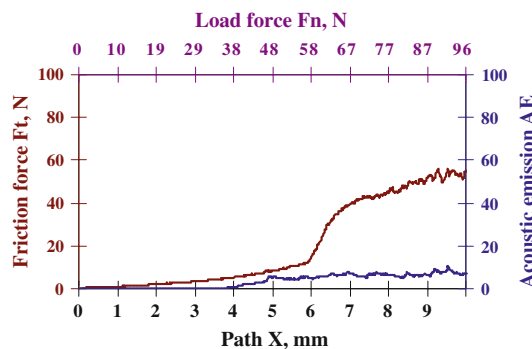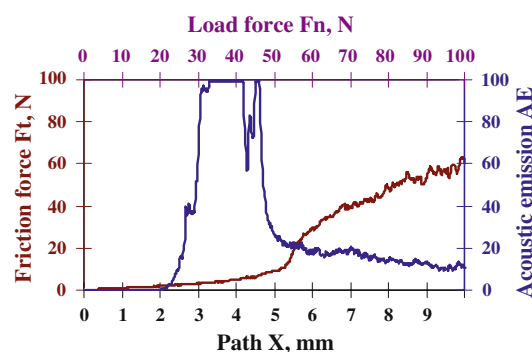
light microscope coupled with a measuring device, thus determining the value of the L_{C1} and L_{C2} critical load on the basis of metallographical observations. In case of the coatings examined, it was found that coating AlTiCrN had the highest critical load value $L_{C1} = 24$ N and $L_{C2} = 54$ N deposited on substrate made of the X40CrMoV5-1 steel, whereas CrAlSiN and TiAlSiN coatings deposited on the substrate made of the X6CrNiMoTi17-12-2 steel had the lowest value. In general, the coatings deposited on the substrate made of the X40CrMoV5-1 hot work tool steel show better adherence to the substrate than coatings deposited on the substrate made of the X6CrNiMoTi17-12-2 austenitic

Table 2 The characteristics of the tested coatings

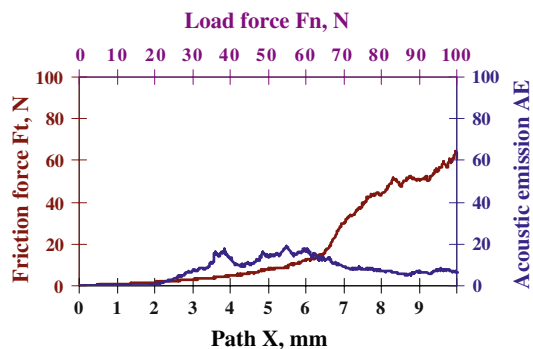| Coating	Thickness (μm)	Microhardness (GPa)	Crystallite size (nm)	Critical load L_{C1} (N)		Critical load L_{C2} (N)	
				AS	HWTS	AS	HWTS
AlTiCrN	2.4	42	17	15	24	27	54
CrAlSiN	2.9	40	25	8	18	28	49
TiAlSiN	2.1	40	11	9	16	27	46

AS austenitic steel, *HWTS* hot work tool steel

Fig. 10 Diagram of the dependence of the acoustic emission (AE) and friction force F_t on the load for the X40CrMoV5-1 steel with the TiAlSiN coating
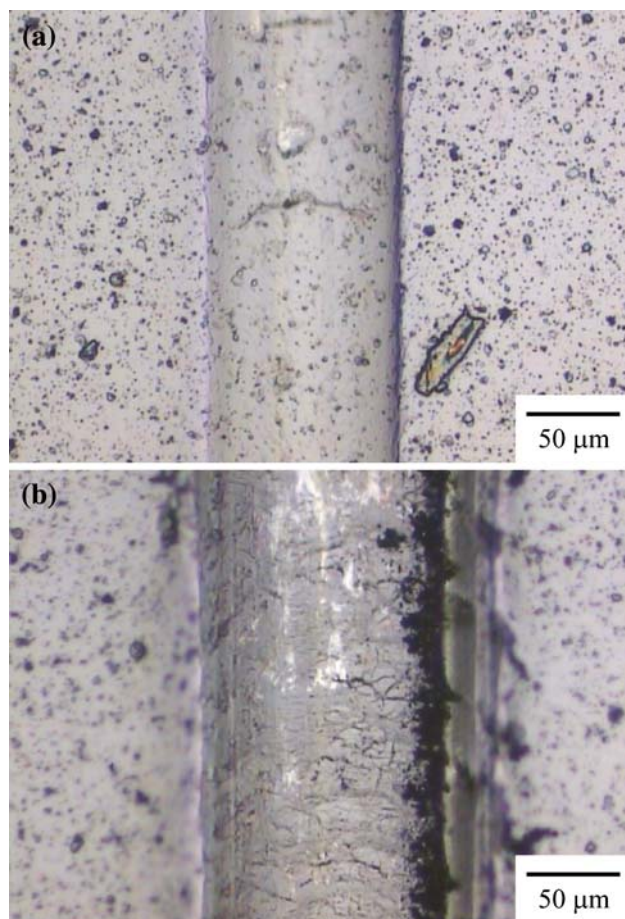

Fig. 11 Scratch failure pictures of the AlTiCrN coating on X40CrMoV5-1 steel substrate at: **a** L_{C1}, **b** L_{C2}

Fig. 12 Scratch failure pictures of the CrAlSiN coating on X40CrMoV5-1 steel substrate at: **a** L_{C1}, **b** L_{C2}

steel. This is caused by a significantly higher hardness of the X40CrMoV5-1 steel.

The first symptoms of damage in most of the coatings examined are in the form of arch cracks caused by tension or scaling occurring on the bottom of the scratch that appears during the scratch test (Figs. 11, 12, 13). Occasionally, there are some small chippings on the scratch
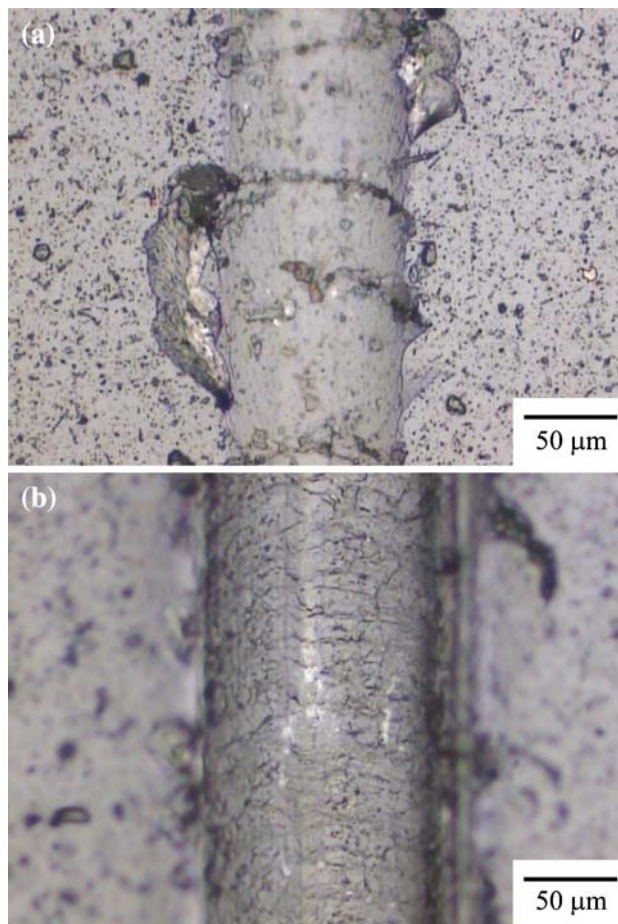
edges. Along with the load increase, semicircles are formed caused by conformal cracking, leading to delaminations and chippings, resulting in a local delamination of the coating. As a result of the steel fracture test against the coatings deposited, made after prior cooling in liquid nitrogen, no case delaminations were revealed along the substrate-coating separation surface, which indicates a good adhesion of coatings to substrate.

Changes of coating component concentration and substrate material made in GDOS were presented in Figs. 14, 15, and 16. The tests carried out with the use of GDOS indicate the occurrence of a transition zone between the substrate material and the coating, which results in the improved adhesion between the coatings and the substrate. In the transition zone between the coatings and the substrate, the concentration of the elements of the substrate increases with simultaneous rapid decrease in concentration of elements contained in the coatings. The existence of the transition zone should be connected with the increase in desorption of the substrate surface and the occurrence of defects in the substrate and the relocation of the elements
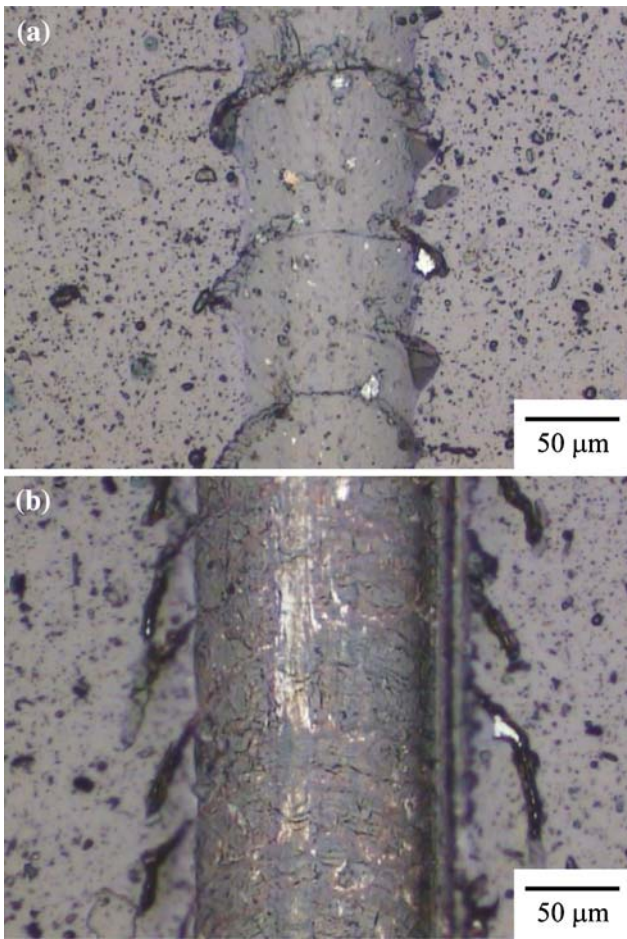
Fig. 13 Scratch failure pictures of the TiAlSiN coating on X40CrMoV5-1 steel substrate at: **a** L_{C1}, **b** L_{C2}
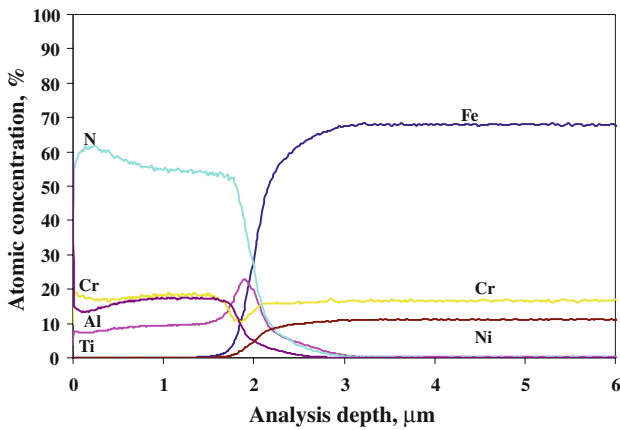

Fig. 14 Changes of constituent concentration of the AlTiCrN and the substrate materials

within the connection zone as a result of a high energy ion reaction. Such results, however, cannot be interpreted explicitly, due to the non-homogeneous evaporation of the material from the sample surface.
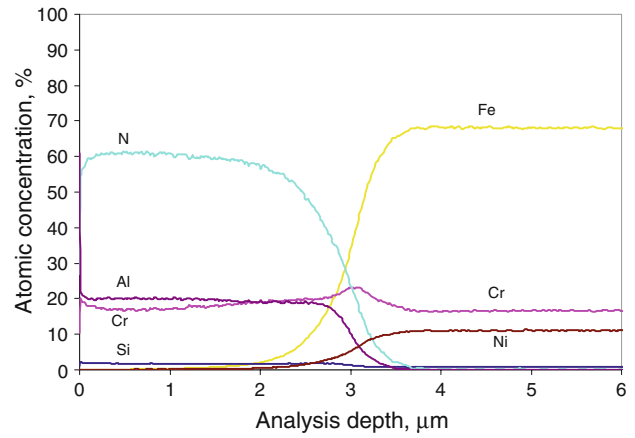

Fig. 15 Changes of constituent concentration of the CrAlSiN and the substrate materials
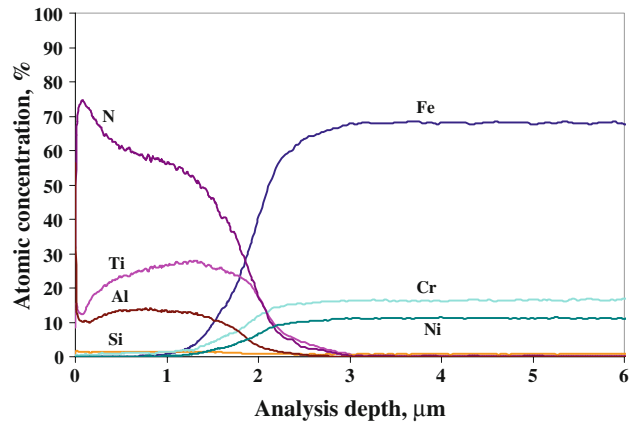

Fig. 16 Changes of constituent concentration of the TiAlSiN and the substrate materials

The corrosion resistance test results of coatings deposited on substrate made of the X6CrNiMoTi17-12-2 austenitic steel with the method of potentiodynamic polarization curves in 1-M HCl solution were presented in Fig. 17. It was found out, as a result of the electrochemical corrosion investigations, that the coatings deposited by PVD process onto the substrate made of the X6CrNiMoTi17-12-2 steel may be an effective substrate material protection against corrosive agents. The potentiodynamic polarization curve analysis (Fig. 17) and that of the corrosion rate confirm the better corrosion resistance of the samples with coatings layers than the uncovered sample (Table 3). During the anode scanning, the current density is always lower for the sample with a coating deposited on its surface in comparison to the uncovered sample (11.56 $\mu A/cm^2$), which indicates a good protective effect. The potentiodynamic polarization curve course is the evidence of the active process of the uncoated X6CrNiMoTi17-12-2 steel surface. The lowest corrosion current density of the
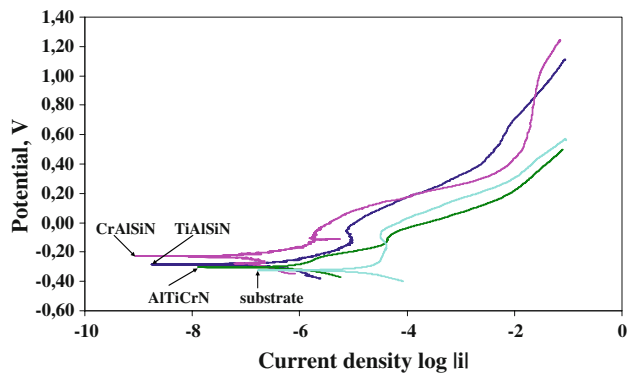
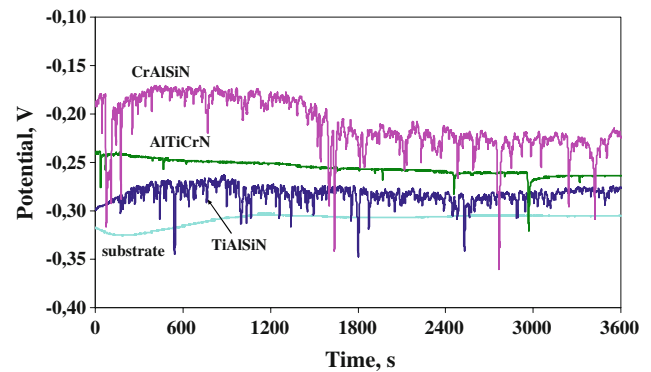**Fig. 17** Potentiodynamic polarization curves of the coatings in 1-M HCl solution

Fig. 18 Open circuit potential curves of the coatings in 1-M HCl solution

Table 3 Summary results of the electrochemical corrosion investigation

Coating type	Current density i_{cor} ($\mu A/cm^2$)	Corrosion potential E_{cor} (mV)	Corrosion rate (mm/year)
AlTiCrN	0.77	−0.26	9.0
CrAlSiN	0.15	−0.22	1.7
TiAlSiN	0.48	−0.28	5.6
Substrate	11.65	−0.30	136.2

Fig. 19 Effect of the electrochemical corrosion on the TiAlSiN coating

investigated coatings is obtained (from Tafel plot) for the CrAlSiN coating. This can be explained by the relatively low porosity of this coating. The current density for the other coatings is significantly higher than the one obtained for the CrAlSiN coating. The shape of the curves in the cathode range indicates the strong slowing down of reactions occurring on the coated samples. The behaviour of the systems tested within the anodic range may evidence the porosity or defect of the coatings. Some of the coatings tested within the anodic range were subjected to self-passivation; however, the passive state occurs within a narrow range of the potentials. The growth of the anodic current related to the transpassivation was observed within the 0–0.4 mV potential range. The corrosion current density and corrosion rate were estimated according to the potentiodynamic curve courses (Table 3). The corrosion potential E_{cor} test results confirm the better corrosive resistance of the coatings (Fig. 18) than the uncoated steel samples. The fact that the corrosive potential of the uncoated substrate significantly grows after a 60-min experiment is also worth noting.

Changes of the coating colour and increase in their roughness caused by the intensive dissolving of their surface were observed during the aggressive agent action (Fig. 19). Microscope observations make it possible to state that the coating damage process due to electrochemical corrosion proceeds in double way. In the first case, the
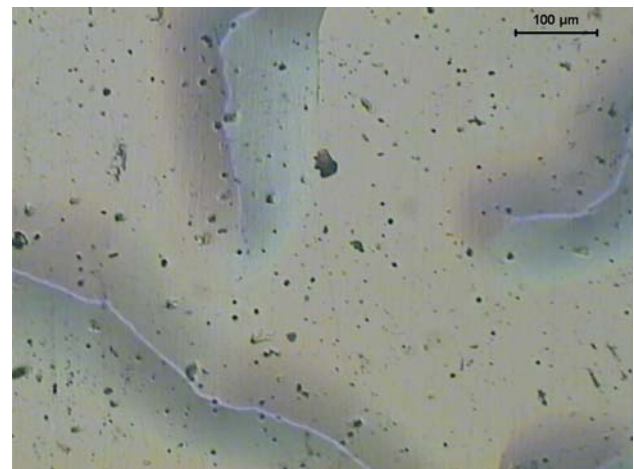
coating damage develops in many places, whereas the area of these damages is small. In the second case, however, the coating damage caused by the aggressive agent action comprises a big area, leading to changes in its appearance or delamination of the coating parts from the substrate material. The tests show pitting corrosive attacks.

Summary

The compact structure of the coatings without any visible delamination was observed in the scanning electron microscope. The fracture morphology of the coatings tested is characterized with a dense structure. Based on the thin film test in the transmission electron microscope, it was observed that the coatings are built of fine crystallites. Their size is 11–25 nm.

The scratch tests on coating adhesion reveal the cohesive and adhesive properties of the coatings deposited on the substrate material. In virtue of the tests carried out, it

was found that the critical load L_{C2} fitted within the range 46–54 N for the coatings deposited on a substrate made of hot work tool steel X40CrMoV5-1 and 27–28 N for coatings deposited on the substrate made of the X6CrNiMoTi17-12-2 austenitic steel. The coatings deposited on the substrate made of the X40CrMoV5-1 steel present a better adhesion than the coatings deposited on the substrate made of the X6CrNiMoTi17-12-2 steel. This is caused by a better hardness of the X40CrMoV5-1 steel. The tests made with the use of GDOS indicate the occurrence of a transition zone between the substrate material and the coating, which affects the improved adhesion between the coatings and the substrate.

As a result of the potentiodynamic polarization curve analysis, the corrosion current density–corrosion rate was determined. It confirms the better corrosion resistance of samples coated with the use of the PVD technique to the uncoated samples made of the austenitic steel (11.65 μA/cm^2). The corrosion current density for the coatings tested fits within the range 0.15–0.77 μA/cm^2, which proves their good anti-corrosion properties.

References

1. Yu C, Wang S, Tian L, Li T, Xu B (2009) J Mater Sci 44:300. doi:10.1007/s10853-008-3066-3
2. Cheng JB, Liang XB, Xu BS, Wu YX (2009) J Mater Sci 44:3356. doi:10.1007/s10853-009-3436-5
3. Kao WH (2009) J Mater Sci 44:3488. doi:10.1007/s10853-009-3467-y
4. Mao Z, Ma J, Wang J, Sun B (2009) J Mater Sci 44:3265. doi:10.1007/s10853-009-3438-3
5. Sundararajan G, Sudharshan Phani P, Jyothirmayi A, Gundakaram RC (2009) J Mater Sci 44:2320. doi:10.1007/s10853-008-3200-2
6. Dobrzanski LA, Lukaszkowicz K, Zarychta A, Cunha L (2004) J Mater Process Technol 164–165:816
7. Lukaszkowicz K, Dobrzanski LA (2008) J Mater Sci 43:3400. doi:10.1007/s10853-008-2523-3
8. Voevodin AA, Zabinski JS, Muratore C (2005) Tsinghua Sci Technol 10:665
9. Yang SM, Chang YY, Wang DY, Lin DY, Wu WT (2007) J Alloys Compd 440:375
10. Tjong SC, Chen H (2004) Mater Sci Eng 45:1
11. Zhang S, Ali N (eds) (2007) Nanocomposite thin films and coatings. Imperial College Press, London
12. Veprek S, Veprek-Heijman MGJ, Karvankova P, Prochazka J (2005) Thin Solid Films 476:1
13. Donnet C, Erdemir A (2004) Surf Coat Technol 180–181:76
14. Voevodin AA, Zabinski JS (2005) Compos Sci Technol 65:741
15. Holubar P, Jilek M, Sima M (2000) Surf Coat Technol 133–134:145
16. Rafaja D, Poklad A, Klemem V, Schreiber G, Heger D, Sima M (2007) Mater Sci Eng A 462:279
17. Carvalho S, Ribeiro E, Rebouta L, Tavares C, Mendonca JP, Caetano Monteiro A, Carvalho NJM, De Hosson JThM, Cavaleiro A (2004) Surf Coat Technol 177–178:459
18. Veprek S (1997) Surf Coat Technol 97:15
19. Veprek S (1998) Thin Solid Films 317:449
20. Rafaja D, Poklad A, Klemm V, Schreiber G, Heger D, Sima M, Dopita M (2006) Thin Solid Films 514:240
21. Burnett PJ, Rickerby DS (1987) Thin Solid Films 154:403
22. Bellido-Gonzalez V, Stefanopoulos N, Deguilhen F (1995) Surf Coat Technol 74–75:884
23. Holmberg K, Matthews A (1994) In: Dowson D (ed) Coatings tribology, vol 1. Elsevier, Amsterdam, pp 264–268
24. Behera SK, Sahu PK, Pratihar SK, Bhattacharyya S (2004) Mater Lett 58:3710
25. Sergici AO, Randall NX (2006) Adv Mater Process 4:1
26. He Y, Apachitei I, Zhou J, Walstock T, Duszczyk J (2006) Surf Coat Technol 201:2534